

<https://doi.org/10.1038/s43247-025-02259-4>

# A warming pulse in the Antarctic continent changed the landscape during the Middle Ages

Check for updates

Emanuele Forte <sup>1</sup>, Maurizio Azzaro <sup>2</sup>, Nicoletta Cannone <sup>3,4</sup>, Alessandro Longhi <sup>3,4</sup>,  
Iliaria Santin <sup>1,5,6</sup> & Mauro Guglielmin <sup>3,4</sup> ✉

The Antarctic landscape is one of the most stable environments on the Earth, at least since approximately 14 million years ago when most glaciers in continental Antarctica changed from temperate to cold-based, and previous extensive fluvial activity disappeared. Here, we detected a large landscape change on a coastal glacier in continental Antarctica (Boulder Clay Glacier) that occurred in the Medieval Warm Period. Such change consists in a glacial unconformity marked by a continuous sediment layer and an erosion channel on the past glacier surface. This channel, more than 4 kilometers long, represents a local deepening of a glacial unconformity that cuts the underlying glacial strata and was clearly imaged and mapped by Ground Penetrating Radar data. Four boreholes were allowed to calibrate the sediment layer so identified because it was observed in all boreholes at depths between 1.85 and 3.07 m. Moreover, the occurrence at a depth of 11.11 meters of mosses suitable for the dating through radiocarbon dating provided the age of 1050 calibrated years before the present, implying that the erosion event occurred during the Medieval Warm Period between 900 and 989 before the present.

The Antarctic landscape is considered to be one of the most stable environments on the Earth, at least since 13.6 Ma (e.g. refs. 1,2.) when most glaciers in the continental Antarctica switched from temperate to cold-based<sup>3-7</sup> and the previous extensive fluvial activity disappeared, except in the McMurdo Dry Valleys where ephemeral streams, or alluvial fans on debris-covered glaciers or rock glaciers are still observed<sup>8-12</sup>. Climate change in the Dry Valleys has triggered rapid landscape changes<sup>13-16</sup>. These changes were mainly due to the fluvial action associated with glacial melting triggered by extreme climatic events, although thickening of the active layer also sometimes caused significant mass movements and surface changes<sup>14-16</sup>. Abrupt modifications of the glacier surface were less common, except for their retreat or thinning.

The occurrence of running water in continental Antarctica was first observed on the Nansen Ice Shelf (northern Victoria Land, not far from our study area) in 1909<sup>17</sup>. Recently, persistent drainage networks that have been active for more than a century have been documented, draining much of the ice shelf's meltwater into the ocean<sup>18</sup>. The presence of meltwater generating surface streams and ponds on the ice sheet has been reported in different regions of continental Antarctica up to 85° S and as high as 1300 m above sea

level (asl), especially close to rocky outcrops or around debris accumulation areas<sup>19</sup>. However, during the ongoing warming, the meltwater runoff was insufficient to transport significant volumes of sediment on the Wright Lower and Canada Glaciers, where a large amount of supraglacial sedimentation persisted on the ice<sup>14,20</sup>.

Here, we demonstrate for the first time, to the best of our knowledge, that an unprecedented palaeo-erosion event occurred on the surface of an Antarctic glacier (northern Victoria Land, continental Antarctica) during the Medieval Warm Period (MWP) between 900 and 989 cal BP, producing a glacial unconformity and a continuous sediment layer above it, as well as a supraglacial erosion channel extending over more than 4 km.

## Results

The evidence of the palaeo-erosion event was obtained from GPR surveys and boreholes performed on the West-East flowing Boulder Clay Glacier (BCG, 74°S, Fig. 1), located about 6 km far from the Mario Zucchelli Antarctic Station (MZS) at mean average elevation of about 220 m asl.

Analysis of the processed GPR data, integrated by specific phase, frequency, amplitude, and texture attributes, imaged several internal

<sup>1</sup>Department of Mathematics, Informatics and Geosciences, University of Trieste, Trieste, Italy. <sup>2</sup>Institute of Polar Sciences, National Research Council (ISP-CNR), Spianata San Raineri, Messina, Italy. <sup>3</sup>Department of Theoretical and Applied Sciences, Insubria University, Varese, Italy. <sup>4</sup>Climate Change Research Center, Insubria University, Varese, Italy. <sup>5</sup>Laboratory of Hydraulics, Hydrology and Glaciology (VAW), ETH, Zurich, Zurich, Switzerland. <sup>6</sup>Swiss Federal Institute for Forest, Snow and Landscape Research (WSL), Birmensdorf, Switzerland. ✉e-mail: [mauro.guglielmin@uninsubria.it](mailto:mauro.guglielmin@uninsubria.it)

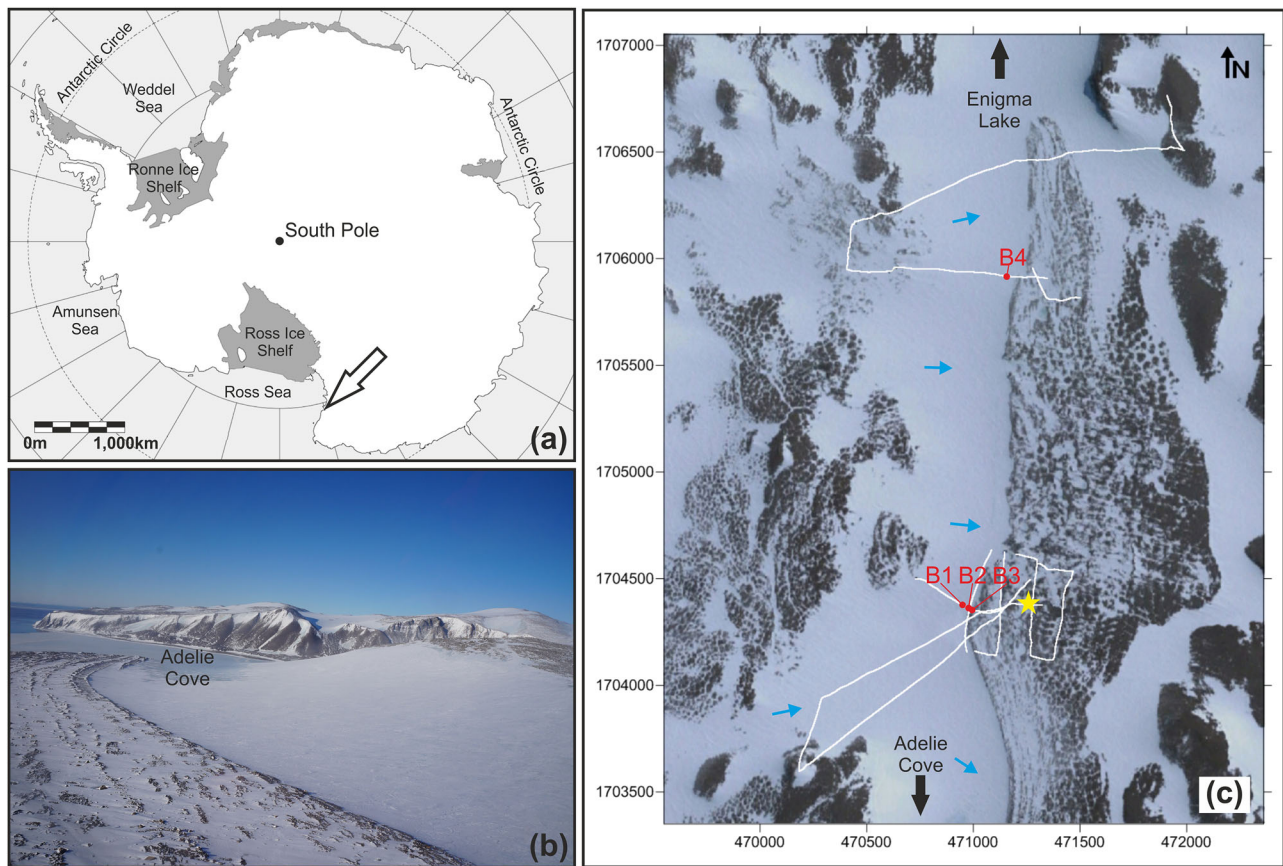


**Fig. 1 | Location map of the study area.** (a) Location map of the study area; (b) view of Boulder Clay Glacier (BCG); (c) georeferenced satellite image with the location of GPR profiles superimposed (continuous white lines). Red dots mark the borehole locations (B1, B2, B3, B4), while light blue arrows (reported from<sup>47</sup>) highlight the flow of the glacier. The yellow star indicates the location of the frost mound dated 790

and 1070 Cal yr BP. The (a) was obtained by the open source Generic Mapping Tools —GMT, release: GMT 5.1.2 <http://gmt.soest.hawaii.edu/projects/gmt> while the (c) has been produced using: Basemap © Google, Maxar Technologies (photograph taken on 4th November 2014).

structures of the BCG (Figs. 2, S1, S5). Beneath a few metres of snow, firn and ice (U1 and U2 limited below by the light blue dashed line and U3), there is a glacial unconformity consisting of a sub-horizontal stratified level characterised by a high-reflective continuous horizon (red dashed line), followed by many dipping reflectors (yellow dashed lines), at the base of which high amplitude reflectors and diffractors marked the presence of the frozen till (dark blue dashed line). The glacial unconformity was located between sub-horizontal shallow levels almost parallel to the actual BCG surface and the dipping reflectors just below. The unconformity was clearly identified on all GPR profiles (Fig. 3) at a depth increasing from approximately 1 to 4 metres to the south. Detailed analysis of the GPR data also imaged an incision with a channel shape at the same boundary, 6 to 9 m wide, close to the actual surface moraine of BCG (Fig. 3).

Comparison between GPR and borehole data (Fig. 4) confirmed the presence of the glacial unconformity, which corresponds to a 4 cm thick graded sediment deposit (Figs. S2, S3) at 2.43 m from the surface in the borehole B1, and to a sandy layer at 3.03 m in B2 (Figs. 4a, S3), where the samples D1a and D2 were selected for radiocarbon dating respectively. The grain size of the two levels is quite different because the former referred to the glacial unconformity was mainly composed by gravel (75%) with 25% of sand (mainly coarse) while the latter, located in the middle of the channel, is composed only by sand (mainly fine) indicating different depositional conditions (Fig. S3). In both cases, the low organic content (0.8% of the material finer than 2 mm, Table 1) and the paucity of the finer fraction did not allow reliable radiocarbon dating.

In the sample D1a the lithology of the clasts is predominantly composed by paragneiss of the Wilson Metamorphic Complex (about 40%) and secondarily by granites and diorites (about 22% each) of the Granite Harbour Formation<sup>21</sup>. Clasts larger than 1 cm revealed the presence of 33% sub-rounded clasts and about the same amount of sub-angular clasts, but also the occurrence of few ironstone and angular clasts.

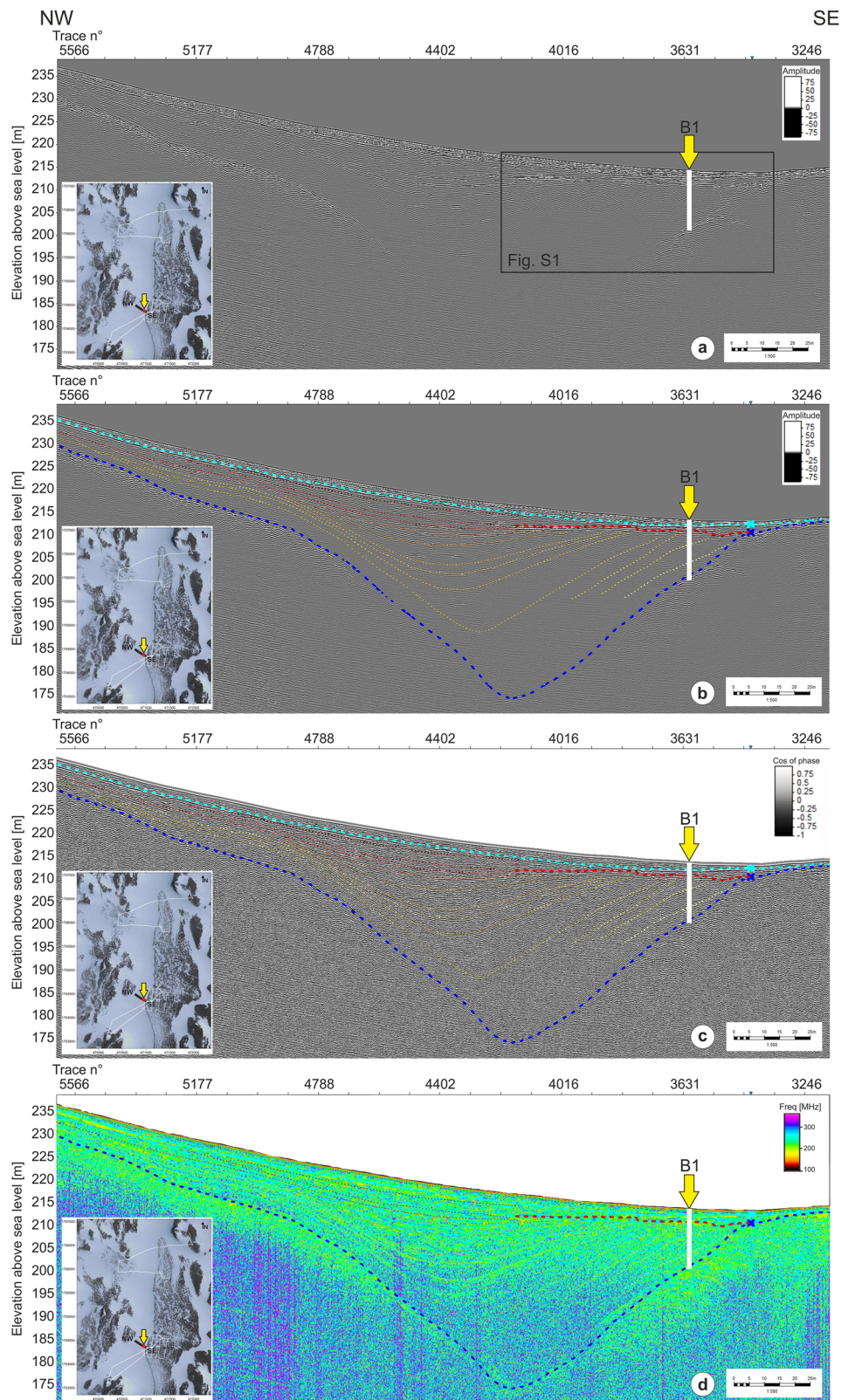
As deduced by the geophysical data and confirmed by the analysis of ice cores (Figs. S4, S5) this horizon has a geometry completely different from the layering just below: it separates the ice of unit U3 (above) from the dipping layered ice of units U4–U8 (Figs. S1, S4).

The absence of nearby Mt. Melbourne volcanic rocks (which are quite common in the till of the adjacent debris-covered glacier) suggests that it is not the source of the sediments found in the channel developed on the glacier and in the horizon along the unconformity. Sample D2 was dominated by sand (80%) and fine gravel, like what was observed in boreholes B3 and B4. As both samples collected along the erosion surface (D1a and D2, Fig. 4a) did not contain any terrestrial macrorests, the <sup>14</sup>C dating was only performed on the sample D1b, which is located below the erosion surface at a depth of 11.18 m (borehole B1) and contains macrorests of mosses along with a layer of some dispersed debris, also detected by GPR (Fig. 4a).

The age of the mosses embedded in the glacier ice in sample D1b was between 956 and 1178 cal BP (Table S1), providing the maximum age for the erosional event that created the glacial unconformity and the channel.

The sample D1b included two different moss species (Fig. S6). The first moss was a sterile gametophyte of *Bryum pseudotriquetrum* (Hedw.) P. Gaertn., while the second one was a sterile gametophyte of *Pohlia nutans*

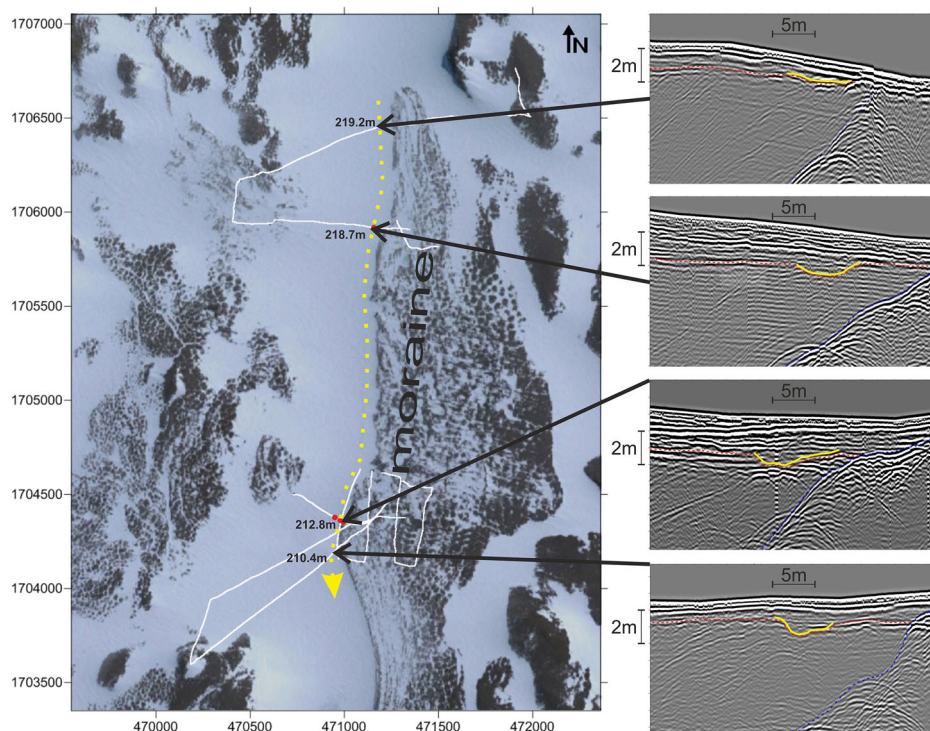
**Fig. 2 | Example of GPR data and of its analyses and interpretation.** Portion of interpreted GPR profile SE-NW crossing the BCG. **a** Processed reflection amplitude; **b** interpreted reflection amplitude; **c** interpreted cosine of instantaneous phase attribute; **d** interpreted dominant frequency attribute. Location of Borehole B1 is marked by the yellow arrow and the white bar. Light blue, red and dark blue dashed lines mark the base of firm, the glacial unconformity and the till, respectively. All the other dashed lines depict the most apparent layers within the glacier. Vertical exaggeration 1.5x.



(Hedw.) Lindb. The first moss sample consisted of a stem about 13 mm long with several leaves with the following characteristics: leaves undifferentiated, ovate-lanceolate to lanceolate, acute, with narrow costa, greenish, yellowish and partly still observable the reddish leaf base, with elongated leaf apex with costa along the all leaf length, not excurrent and with leaves clearly bordered. These characteristics allowed to identify the genus as *Bryum* and, among the

Antarctic species of the genus *Bryum*, the sample was identified as *B. pseudotriquetrum* because of its erect or ascending stem, plant not silvery, lack of gemmae or bulbils with costa relatively strong, percurrent and leaves often cuspidate. *B. archangelicum* and *B. pallescens* were excluded according to Cannone et al.<sup>22</sup>, as the Antarctic samples of these species were all recognised as *B. pseudotriquetrum*.

**Fig. 3 | Reconstruction of the path of the erosion channel along the glacial unconformity at Boulder Clay Glacier.** Reconstruction of the path of the erosion channel (yellow dotted line on the left). On the right portions of GPR profiles from North to South imaging the channel (yellow solid line) and the glacial unconformity (red dotted line), both cutting the underlying dipping glacial strata. Red dots mark the borehole locations, while elevations (m asl) refer to the deepest point of the erosion channel at each location. Blue dashed line follows the top of the till. The left panel has been produced using: Basemap © Google, Maxar Technologies (photograph taken on 4th November 2014).



The second moss sample consisted of a stem about 10 mm long, with several leaves showing characteristics similar to those of the first sample, but with an important difference: the occurrence of leaves not clearly bordered, allowing to identify its genus as *Pohlia* (<sup>23</sup>, p. 418) and, among the species occurring in Antarctica, as *P. nutans* due to the lack of propagules, to the leaves not or weakly decurrent and the costa darker (brownish) at the base.

## Discussion

### Palaeoclimate and landscape changes

At the best of our knowledge, this is the first evidence of past fluvial erosion, sediment transportation and fluvial deposition on a glacier surface in continental Antarctica, despite recently significant amount of meltwater events having been reported for the last century on the East Antarctic Ice Sheet<sup>13</sup> and on the Nansen Ice Shelf<sup>12</sup>.

Our data show that the supraglacial melting was widespread on all the BCG surface, cutting the glacier's strata and creating a glacial unconformity (fig. S8) on which was deposited a graded layer (indicating a progressive decrease of the flow current speed), whereas along the BCG moraine (Fig. 3) the melting erosion carved a channel longer than 4 km. In the channel the erosional event was followed by a depositional event with a decreased current so that only sand was deposited (Fig. 5).

It is also noteworthy that under current climatic conditions, despite some of the effects of recent climate change that have been observed even in continental Antarctica, there is no evidence of meltwater on the BCG, and the surface of the glacier is permanently snow-covered. Therefore, the occurrence of an almost ubiquitous glacial unconformity within the BCG and the development of a long fluvial channel (more than 4 km) as illustrated in Fig. 5 indicate exceptional climatic conditions in the BCG area.

When did such an event occur? What could have caused this peculiar situation? The age of the sample D1b (ca. 1050 cal BP) predates the erosion and depositional event documented by the sediment layer marking the unconformity. Indeed, considering the past surface mass balance (SMB) in this Antarctic sector we can reasonably assume an accumulation rate between 7 and 25 cm of ice per year<sup>24,25</sup> and therefore, the fluvial erosion and supraglacial-fluvial sedimentation event at BCG is likely to have occurred at least between 35 to 125 years after the deposition of the mosses, dated

around 1050 cal BP (956–1178 cal BP, Table 1). Therefore, according to the possible different accumulation rates in the BCG, the event occurred between 831 and 1140 cal BP.

Moreover, D1b can be considered a reliable sample due to the fairly good preservation status of the moss stems (Fig. S6), which confirms their sin-sedimentary deposition relative to the snow that formed the ice layer.

The moss species within the ice core are two species that occur on Victoria Land. In particular, *Bryum pseudotriquetrum* (Hedw.) P. Gaertn. is one of the most widespread mosses in Antarctica with several locations recorded in Victoria Land<sup>26,27</sup>. Its occurrence within the ice core is compatible with environmental and climatic conditions like the present. A more surprising discovery is *Pohlia nutans* (Hedw.) Lindb., which is very rare in continental Antarctica and in Victoria Land, where it has only been observed associated with the fumaroles of active volcanoes (Mt. Rittmann and Mt. Melbourne)<sup>28–30</sup>.

The occurrence of *P. nutans* may be related to passive transport by winds from the active volcanic fumaroles of Mt. Melbourne (located approximately 50 km north of BCG) and/or of Mt. Rittmann (located at > 100 km northwest of the study site). Winds have been generally identified as one of the most likely dispersal agents of the Antarctic moss flora<sup>31,32</sup>, which may occur across long distances, as also confirmed in northern Victoria Land by the occurrence of pollen grains in moss cushions<sup>33</sup>. The occurrence of *P. nutans* could be likely explained also by hypothesizing warmer palaeoclimatic conditions allowing its persistence outside the volcanic fumaroles, as happens nowadays in maritime Antarctica<sup>23,28</sup>.

The period between 831 and 1140 cal BP is characterised by reduced sea ice in northern Victoria Land<sup>34</sup>, which is consistent with the occurrence of a brief event of warmer conditions around 1000 cal BP, further supported by the observation of a monospecific flora of *Corethron criophilum* in the Granite Harbour area<sup>35</sup>.

Terrestrial records indicate that the MWP affected the landscape in northern Victoria Land as confirmed by the regression of the Edmonson Point Glacier (about 50 km North of the study area) dated between 900 and 1030 cal BP<sup>36</sup>. Further support for the occurrence of this short warming period was provided by the largest uplift event for the frost mound in the lake 16 (yellow star in Fig. 1)<sup>37,38</sup>, observed only few hundred metres from

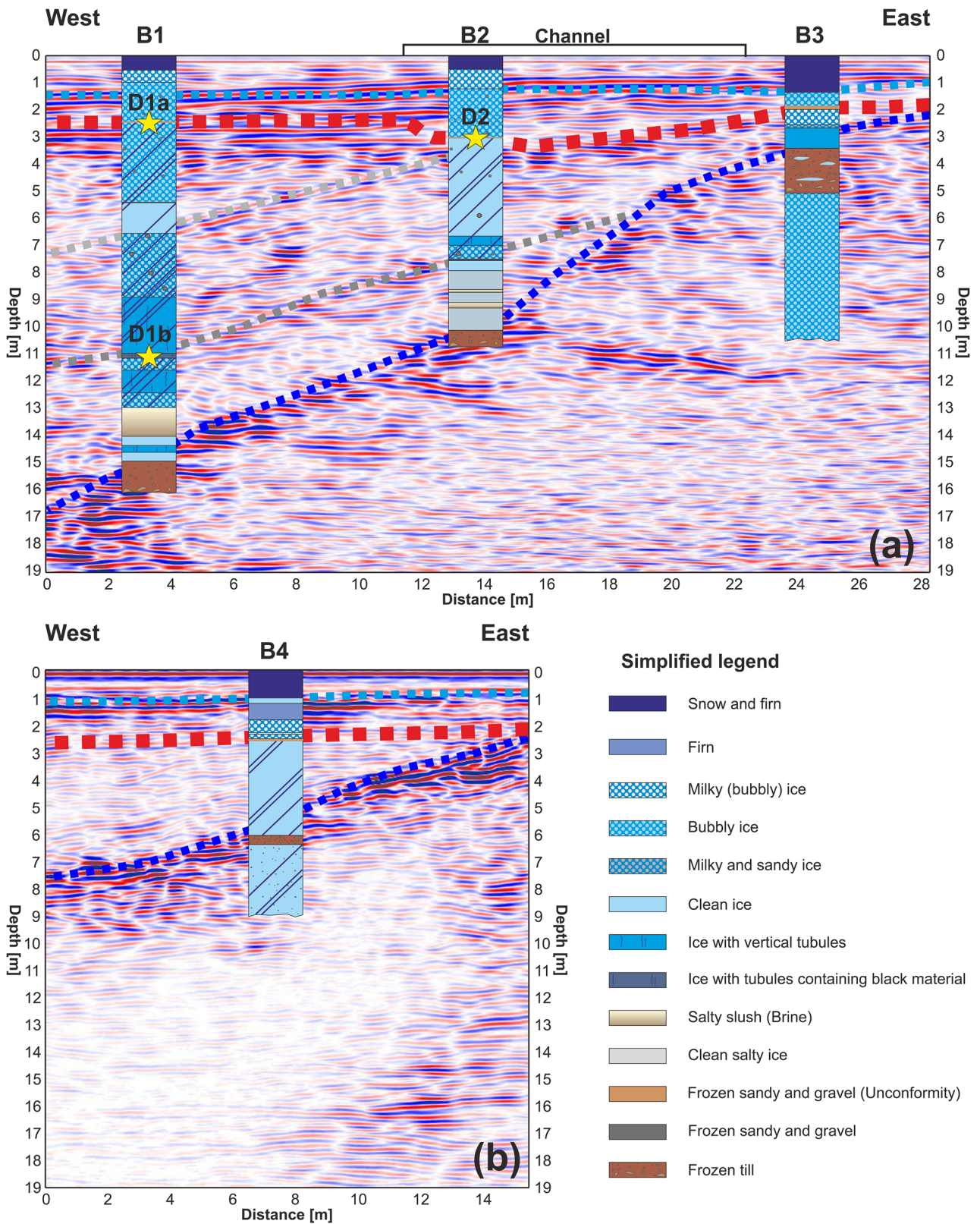


**Fig. 4 | Relations between GPR profiles and borehole stratigraphies.** Relations between GPR profiles and boreholes: (a) South transect with the boreholes B1, B2 and B3; (b) Northern transect with borehole B4. Dotted lines indicate the main surfaces revealed by the GPR (from the top to the bottom: light blue = contact

between snow-firn and ice; red = glacial unconformity (erosion surface); gray = debris bands embedded in the ice; brown = contact between glacial ice and till. Yellow stars indicate the locations of samples analysed to find macrorests for <sup>14</sup>C dating.

**Table 1 | Geomorphological location and main characteristics of the samples considered for radiocarbon dating**

	D1a	D2	D1b
Location	Glacial Unconformity	Channel	Debris band embedded in ice
Borehole	B1	B2	B1
Depth (m)	2.43	3.03	11.18
Gravel (%)	76	0	15
Sand (%)	24	99	5 (silt and clay, =80%)
Ironstone	Yes	No	N.D.
Organic Mat (%)	0.8	0.7	22
Macrorests	No	no	mosses

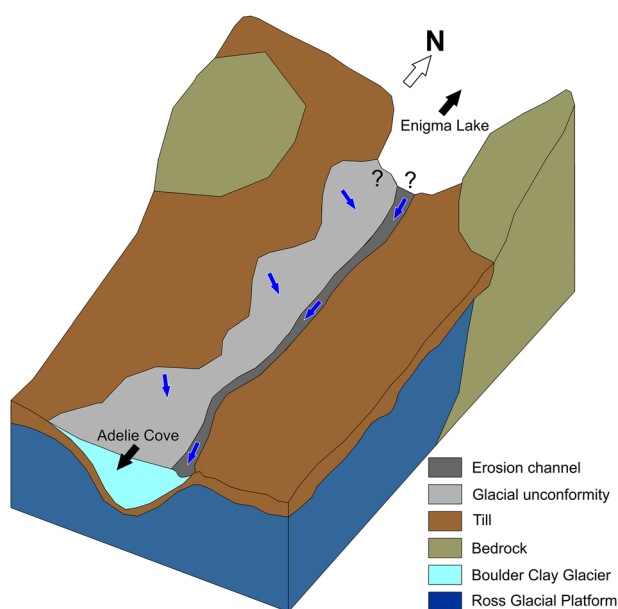


**Fig. 5 | Scheme of the extent and spatial behaviour of the erosion channel and the glacial unconformity at Boulder Clay Glacier.** The scheme illustrates the spatial distribution of the erosion features developed during the Middle Ages in the study area respect to the surrounding glacial environment and the bedrock. It is remarkable as the glacial unconformity (grey surface) involved the whole glacier. Data from<sup>48</sup> have also been considered, particularly as far as the Ross Glacial Platform.

borehole B1 and dated between 790 and 1070 cal BP<sup>39</sup>. The uplift of the frost mound is caused by a combination of extensive summer melting followed by severe winter freezing<sup>38</sup>. Therefore, the past frost mound uplift documented at BCG may indicate that the summer melt during the MWP was greater than today.

The MWP in Victoria Land has been reported to be mainly driven by the El Niño-Southern Oscillation (ENSO)<sup>40</sup>, which is linked to changes in solar activity through non-linear dynamics<sup>24</sup>.

In terms of atmospheric temperature, the most representative proxy for this area is probably the isotopic record obtained at Talos Dome, known as TALDICE<sup>34,41</sup>. The TALDICE δ<sup>18</sup>O isotopic record (Fig. 6) shows three maxima at 837, 906 and 989 cal BP.

Therefore, considering all the evidence for warming (Fig. 6), it is reasonable to assume that the water erosion and supraglacial-fluvial sedimentation event on BCG could be dated between 900 and 989 cal BP, consistent with the MWP. The results presented here show that even in continental Antarctica, at least on the Boulder Clay Glacier, a huge warm pulse event with major landscape changes in the pre-industrial era has been recorded.

## Methods

### GPR data acquisition, processing and analysis

GPR datasets were collected on the BCG in November 2014 and 2017 using a ProEx Malå Geoscience GPR, equipped with 250 and 500 MHz shielded antennas, with a constant offset equal to 0.31 and 0.18 m, respectively. A GPS (Thales Magellan Promark 3) was used for absolute positioning, while the GPR was triggered by an electromechanical odometer connected to the antennas. The trace interval was 0.10 m, while the sampling interval was equal to 0.399 and 0.186 ns, for 250 and 500 MHz antennas respectively. The vertical stacking was set to 8. The transmitting and receiving antennas were parallel to each other and transverse to the survey direction, which minimises offline reflections.

GPR data were processed using ProMAX software (Halliburton) originally developed for reflection seismics datasets, with a processing flow that includes drift removal (zero-time correction), background removal (applied in the time domain), topographic (static) corrections, geometrical spreading and amplitude recovery, spectral analysis and filtering and 2D migration (Kirchhoff). We used a simplified EM velocity field for this flow, assuming a velocity of 20 cm ns<sup>-1</sup> for the shallowest layers (firn) and to 17 cm ns<sup>-1</sup> for the ice. Local variations may exist, but considering the absence of free water within the frozen materials (except for brines which have been reported in some parts of the study area by Azzaro et al.<sup>42</sup>, they should be small. We applied a true amplitude approach, avoiding the use of algorithms that could distort or equalise the trace amplitudes, such as automatic gain control functions. In this way, it is possible to obtain amplitudes that, under ideal conditions, are related only to the electrical impedance contrasts of the subsurface, i.e. only to the reflection coefficients.

Given the overall high quality and high signal-to-noise ratio of the processed data, GPR attribute analysis was performed to integrate the basic interpretation of amplitude data with more detailed information on the physical property variations and to classify domains characterised by homogeneous GPR response. Attributes have shown great potential for glaciological applications<sup>43,44</sup> and were used here specifically to highlight lateral horizon continuity and reflector geometry as well as to image peculiar spectral characteristics of the EM signal. Different attribute categories, including amplitude-/phase-/frequency-related, and textural ones, were used to improve the accuracy of data interpretation.

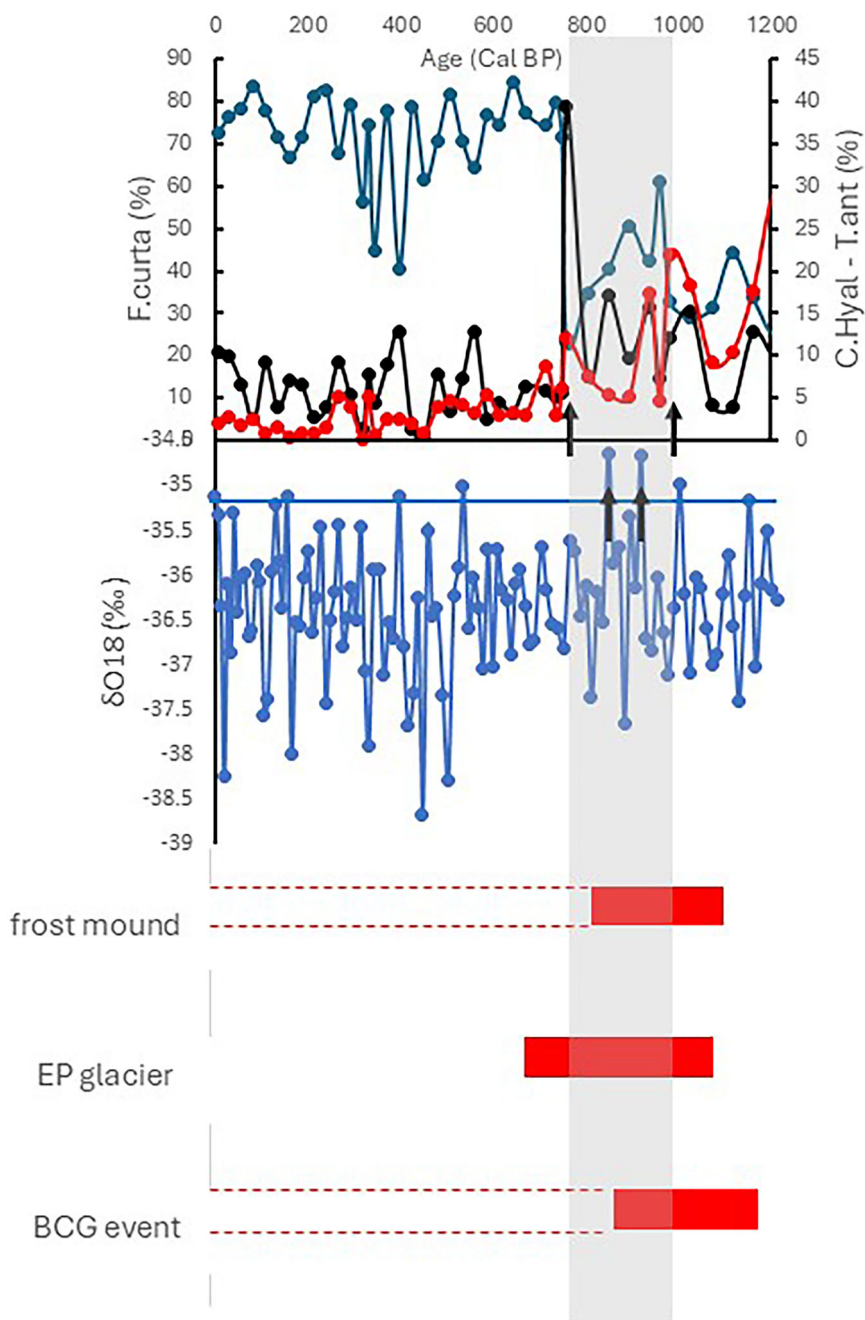
### Ice cores

To calibrate the geophysical survey and describe the glacier cryostratigraphy, we drilled four boreholes (B1 to B4) along the GPR profiles in November 2018 and 2019 with a recovery rate of 98-99%. In particular, three of the cores were located along a West-East transect (B1-B3, Fig. 4a) reaching depths of 16.10, 10.70 and 10.55 m, respectively, while the fourth borehole was located to the north (B4, Fig. 4b) at a depth of 9.10 m. All four boreholes were drilled using a widia bites core auger with compressed and cooled air. The core samples were collected and shipped in a frozen state (-20 °C) to Italy, where they were cut along their longitudinal diameter in a -20 °C room. Core characterisation included the borehole stratigraphy and the description of the ice type (based on bubble density and orientation, and clast content), (Figs. S4 and S5).

### Recommendations for the landscape changes reconstruction through GPR investigations

Our data show the importance of correlating borehole stratigraphy with high resolution GPR surveys. Indeed, only by using a 2.5-D correlation of GPR profiles and dedicated attribute analyses it is possible to highlight the regional importance and significance of the 45 mm thick sediment layer between ice units U3 and U4, which represents the deposition of sediments transported by flowing water on the BCG surface. While coring is essential to understand the details of the layering and the temporal history of the events, GPR data are crucial to discriminate the shallow units (U1 to U3) from the dipping horizons, as well as to define the geometry of the ice bottom. Indeed, by using only core samples it is almost impossible to distinguish the shallow ice (U3), which has a layering sub-parallel to the present

**Fig. 6 | Evidence of warming during the MWP in Northern Victoria Land through different proxies.** Comparison between the available evidence of warming during the MWP in Northern Victoria Land according to the main available terrestrial and marine proxy and our interpreted erosion event with the date at BCG. From the top: Diatoms distribution in the Wood Bay<sup>35</sup>: the two black arrows pointed out two years (758 and 1026 cal BP) in which the *F. curta* strongly decreased and *C. hyal* and *T. antarctica* increased suggesting a sea ice reduction; TALDICE  $\delta O^{18}$ <sup>35</sup>: the two black arrows indicate the warmest years in examined period (837 and 907 cal BP, respectively) while the blue horizontal line indicates the average values of the uppermost part of the ice core dated between 1950 and 1991 AD; frost mound: the red bar shows the calibrated age of the dated sample on the frost mound, which represents the maximum age of a very warm summer when the mound was uplifted<sup>40</sup>; EP glacier: the red bar indicates the period of the glacial retreat recorded at the Edmonson Point Glacier<sup>37</sup>; BCG event: the red bar shows the calibrated age of the BCG event that is the maximum age of our erosional event. The light grey column underlined the period (758-1026 cal BP) where most of the proxies overlap with the BCG dates. The data here reported related to Megzecz et al. (2017) were downloaded by <https://www.ncdc.noaa.gov/paleo/study/22590>.



topographic surface, from the deeper dipping ice units (U4-U8). High-resolution GPR ( $\geq 200$  MHz) GPR surveys certainly have less penetration, but they achieve better resolution, which is essential for a detailed definition of ice stratigraphy, as shown in our case.

**Radiocarbon dating and macrorests identifications**

To date some of the events recorded in the glacier stratigraphy we sampled both ice with sparse sediments and sediment layers and/or macrorests within them. In the shallowest part of the glacier the organic content was too low to yield any results. Sediments along the glacial unconformity and in the alluvial channel were sampled for the dating in the cores B1 and B2, respectively. In both cases no terrestrial macrorests were found (only some shell fragments were found D1a at 2.43 m of depth in the core B1) and therefore the bulk sediments were not dated. At greater depths (specifically between 11.11 and 11.18 m) some terrestrial macrorests (moss stems) were found in B1, allowing an AMS age to be assigned to these materials.

The moss samples were stems and leaves of sterile gametophytes, and their identification was performed based on the observation at the microscope dissector of their morphological characteristics according to the key to the identification of Antarctic mosses provided by Ochrya et al.<sup>23</sup> at the genus and species level, respectively.

Radiocarbon dating was performed by Beta Analytic using AMS analysis after a full acid/alkali/acid pre-treatment to remove carbonates (with a hot HCl acid wash) and to remove secondary organic acids with an alkali wash (NaOH). The alkali wash was followed by a final acid rinse to neutralise the solution before drying. The results were then calibrated with Oxcal 4.4<sup>45</sup> according to the SHCAL20 database<sup>46</sup>.

**Data availability**

The GPR data used in this paper are stored in the public repository Zenodo and are available on request at the following link: <https://zenodo.org/records/6090268>.

Received: 23 September 2024; Accepted: 28 March 2025;  
Published online: 11 April 2025

## References

1. Sugden, D. E. & Denton, G. H. Cenozoic landscape evolution of the Convoy Range to Mackay Glacier area, Transantarctic Mountains: onshore to offshore synthesis. *Geol. Soc. Am. Bull.* **116**, 840–857 (2004).
2. Sugden, D. E. et al. Landscape development in the Royal Society Range, southern Victoria Land, Antarctica: stability since the mid-Miocene. *Geomorphology* **28**, 181–200 (1999).
3. van der Wateren, F. M. & Hindmarsh, R. East Antarctic ice sheet: stabilists strike again. *Nature* **376**, 389–391 (1995).
4. Armienti, P. & Baroni, C. Cenozoic climatic change in Antarctica recorded by volcanic activity and landscape evolution. *Geology* **27**, 617–620 (1999).
5. Lewis, A. R., Marchant, D. R., Ashworth, A. C., Hemming, S. R. & Machlus, M. L. Major middle Miocene global climate change: evidence from East Antarctica and the Transantarctic Mountains. *Geol. Soc. Am. Bull.* **119**, 1449–1461 (2007).
6. Oberholzer, P., Baroni, C., Salvatore, M. C., Baur, H. & Wieler, R. Dating late Cenozoic erosional surfaces in Victoria Land, Antarctica, with cosmogenic neon in pyroxenes. *Antarct. Sci.* **20**, 89–98 (2008).
7. Smellie, J. L. et al. Glaciovolcanic evidence for a polythermal Neogene East Antarctic Ice Sheet. *Geology* **42**, 39–41 (2014).
8. Stuiver, M. et al. History of the marine ice sheet in West Antarctica during the last glaciation: a working hypothesis, in *The Last Great Ice Sheets*, edited by G. H. Denton and T. J. Hughes, pp. 319–362 (John Wiley & Sons, 1981).
9. Dickson, J. L., Head, J. W., Levy, J. S., Marchant, D. R. & Pond, D. o. n. J. u. a. n. Antarctica: Near surface CaCl<sub>2</sub>-brine feeding Earth's most saline lake and implications for Mars. *Sci. Rep.* **3**, 1166 (2013).
10. Kowalewski D. E. et al. Orbital Forcing of High Elevation Meltwater Events along the Periphery of East Antarctica. *AGU Fall Meeting Abstracts*, PPA53A–2308 (2015).
11. Wlostowski, A. N., Gooseff, M. N., McKnight, D. M., Jaros, C. & Lyons, W. B. Patterns of hydrologic connectivity in the McMurdo Dry Valleys, Antarctica: a synthesis of 20 years of hydrologic data. *Hydrol. Process.* **30**, 2958–2975 (2016).
12. Winsor, K. et al. Origin, structure and geochemistry of a rock glacier near Don Juan Pond, Wright Valley, Antarctica. *Antarct. Sci.* **32**, 273–287 (2020).
13. Levy, J. S. et al. Decadal topographic change in the McMurdo Dry Valleys of Antarctica: Thermokarst subsidence, glacier thinning, and transfer of water storage from the cryosphere to the hydrosphere. *Geomorphology* **323**, 80–97 (2018).
14. Fountain, A. G., Levy, J. S., Gooseff, M. N. & Van Horn, D. The McMurdo Dry Valleys: a landscape on the threshold of change. *Geomorphology* **225**, 25–35 (2014).
15. Fountain, A. G. et al. The impact of a large-scale climate event on Antarctic ecosystem processes. *BioScience* **66**, 848–863 (2016).
16. Gooseff, M. N. et al. Decadal ecosystem response to an anomalous melt season in a polar desert in Antarctica. *Nat. Ecol. Evolut.* **1334**, 1334–1338 (2017).
17. David T. W. E. et al. *Geological Observations in Antarctica by the British Antarctic Expedition 1907–1909* (JP Lippincott, 1909).
18. Bell, R. E. et al. Antarctic ice shelf potentially stabilized by export of meltwater in surface river. *Nature* **544**, 344–348 (2017).
19. Kingslake, J. C. E., Ely, J. C., Das, I. & Bell, R. E. Widespread movement of meltwater onto and across Antarctic ice shelves. *Nature* **544**, 349–352 (2017).
20. MacDonell, S. A., Fitzsimons, S. J. & Mölg, T. Seasonal sediment fluxes forcing supraglacial melting on the Wright Lower Glacier, McMurdo Dry Valleys, Antarctica. *Hydrol. Process.* **27**, 3192–3207 (2013).
21. Carnignani L. et al. Geological Map at 1:500,000 scale of the Wilson Terrane in the area between David and Mariner Glaciers, Victoria Land (Antarctica). *Memorie Della Societa' Geologica Italiana*, **33** (1987).
22. Cannone, N., Vanetti, I., Convey, P., Sancho, L. G. & Zaccara, S. Molecular analyses support revision of species diversity of the moss genus *Bryum* in Antarctica. *Bot. J. Linn. Soc.* **XX**, 1–11 (2024).
23. Ochyra R. et al. *The Illustrated Moss Flora of Antarctica*. (Cambridge University Press, 2008).
24. Frezzotti, M., Scarchilli, C., Becagli, S., Proposito, M. & Urbini, S. A synthesis of the Antarctic surface mass balance during the last 800 yr. *Cryosphere* **7**, 303–319 (2013).
25. Winstrup, M. et al. A 2700-year annual timescale and accumulation history for an ice core from Roosevelt Island, West Antarctica. *Climate* **15**, 751–779 (2019).
26. Cannone, N. A network for monitoring terrestrial ecosystems along a latitudinal gradient in continental Antarctica. *Antarct. Sci.* **18**, 549–560 (2006).
27. Cannone, N., Convey, P. & Guglielmin, M. Diversity trends of bryophytes in continental Antarctica. *Polar Biol.* **36**, 259–271 (2006).
28. Bargagli, R. et al. New record of moss and thermophilic bacteria species and physico-chemical properties of geothermal soils on the northwest slope of Mt. Melbourne (Antarctica). *Polar Biol.* **27**, 423–431 (2004).
29. Bargagli, R., Broady, P. A. & Walton, D. W. H. Preliminary investigation of the thermal biosystem of Mount Rittmann fumaroles (Northern Victoria Land, Antarctica). *Antarct. Sci.* **8**, 121–126 (1996).
30. Skotnicki, M. L., Bargagli, R. & Ninham, J. A. Genetic diversity in the moss *Pohlia nutans* on geothermal ground of Mount Rittmann, Victoria Land, Antarctica. *Polar Biol.* **25**, 771–777 (2002).
31. Winkworth, R. C., Wagstaff, S. J., Glenney, D. & Lockhart, P. J. Plant dispersal N.E.W.S. from New Zealand. *Trends Ecol. Evolut.* **17**, 514–520 (2002).
32. Munoz, J., Felicísimo, A. M., Cabzas, F., Burgaz, A. R. & Martinez, I. Wind as a long distance dispersal vehicle in the Southern Hemisphere. *Science* **304**, 1144–1147 (2004).
33. Linskens, H. F., Bargagli, R., Cresti, M. & Focardi, S. Entrapment of long-distance transported pollen grains by various moss species in coastal Victoria Land, Antarctica. *Polar Biol.* **13**, 81–87 (1993).
34. Mezgec, K. et al. Holocene sea ice variability driven by wind and polynya efficiency in the Ross Sea. *Nat. Commun.* **8**, 1334 (2017).
35. Leventer, A., Dunbar, R. B. & DeMaster, D. J. Diatom evidence for Late Holocene climatic events in Granite Harbor, Antarctica. *Paleoceanography* **8**, 373–386 (1993).
36. Baroni, C. & Orombelli, G. Holocene glacier variations in the Terra Nova Bay area (Victoria Land, Antarctica). *Antarct. Sci.* **6**, 497–505 (1994).
37. Ponti, S., Scipinotti, R., Pierattini, S. & Guglielmin, M. The Spatio-Temporal Variability of Frost Blisters in a Perennial Frozen Lake along the Antarctic Coast as Indicator of the Groundwater Supply. *Remote Sens.* **13**, 435 (2021).
38. M. Guglielmin, A. G. Lewkowicz, H. M. French, A. Strini Lake-ice blisters, Terra Nova Bay area, Northern Victoria Land, Antarctica. *Geogr. Ann. Ser. A Phys. Geogr.* **91** (2009) <https://doi.org/10.1111/j.1468-0459.2009.00357.x>.
39. Abramovich, R. S., Pomati, F., Jungblut, A. D., Guglielmin, M. & Neilan, B. A. T-RFLP fingerprinting analysis of bacterial communities in Debris Cones, Northern Victoria Land, Antarctica. *Permafrost. Periglac. Process.* **23**, 244–248 (2012).
40. Lüning, S., Gaika, M. & Vahrenholt, F. The Medieval Climate Anomaly in Antarctica. *Palaeogeogr. Palaeoclimatol. Palaeoecol.* **532**, 109251 (2019).
41. Stenni, B. et al. Expression of the bipolar seesaw in Antarctic climate records during the last deglaciation. *Nat. Geosci.* **4**, 46–49 (2011).

42. Azzaro, M. et al. The prokaryotic community in an extreme Antarctic environment: the brines of Boulder Clay lakes (Northern Victoria Land). *Hydrobiologia* **848**, 1837–1857 (2021).
43. Zhao, W., Forte, E., Colucci, R. R. & Pipan, M. High-resolution glacier imaging and characterization by means of GPR attribute analysis. *Geophys. J. Int.* **206**, 1366–1374 (2016).
44. Santin, I. et al. Recent evolution of Marmolada glacier (Dolomites, Italy) by means of ground and airborne GPR surveys. *Remote Sens. Environ.* **235**, 1–11111442 (2019).
45. Bronk Ramsey, C. Bayesian analysis of radiocarbon dates. *Radiocarbon* **51**, 337–360 (2009).
46. Hogg A. et al., SHCal20 Southern Hemisphere calibration, 0–55,000 years cal BP. *Radiocarbon*. **62**, 759–778 (2020).
47. Baroni, C. Geomorphological map of the Northern Foothills near the Italian station (Terra Nova Bay, Antarctica). *Mem. Soc. Geol. It.* **33**, 195–211 (1987).
48. Forte, E. et al. Evidence of brines interconnections and different flow patterns within the Boulder Clay Glacier and its moraine (Victoria Land, East Antarctica). *Sci. Total Environ.* **957**, 177469 (2024).

## Acknowledgements

This work was supported by grants from the National Antarctic Research Program (PNRA 2013/AZ1.05; PNRA16\_00194; PNRA18\_00186-E). We gratefully acknowledge Schlumberger and Halliburton through their University of Trieste academic grants. We thank also F. Malfasi, S. Ponti, F. Baio, and U. Neumann for their field and lab assistance. A special thanks to Bethan Davies for the kind permission to use her picture in our Fig. S8. We would also like to thank the Associate Editor Prof. Carolina Ortiz Guerrero, the reviewer Prof. Juan-Luis García and an anonymous reviewer for their valuable suggestions that significantly improved the manuscript. Borehole sampling was authorized by ENEA-PNRA according to the environmental Antarctic rules.

## Author contributions

Emanuele Forte Conceptualization (equal); GPR data curation (equal); GPR investigation (equal); formal analysis (equal); methodology (equal); data acquisition and elaboration; funding acquisition (equal); visualization (equal); writing—original draft (equal); writing—review and editing (equal). Maurizio Azzaro Borehole investigation (equal); writing—original draft (equal). Nicoletta Cannone Borehole formal analysis (equal); methodology (equal); visualization (equal); writing—original draft (equal); writing—review and editing (equal). Alessandro Longhi Borehole formal analysis (equal); writing—original draft (equal). Ilaria Santin GPR data curation (equal); GPR investigation (equal); GPR formal analysis (equal); methodology (equal); visualization (equal); writing—original draft (equal); writing—review and editing (equal). Mauro Guglielmin Conceptualization (equal); GPR

investigation (equal); Borehole investigation (equal), Borehole formal analysis (equal); Borehole data curation (equal); methodology (equal); funding acquisition (equal); visualization (equal); writing—original draft (equal); writing—review and editing (equal); Supervision; Corresponding Author.

## Competing interests

The authors declare no competing interests.

## Additional information

**Supplementary information** The online version contains supplementary material available at <https://doi.org/10.1038/s43247-025-02259-4>.

**Correspondence** and requests for materials should be addressed to Mauro Guglielmin.

**Peer review information** *Communications Earth & Environment* thanks Juan-Luis García and the other anonymous reviewer(s) for their contribution to the peer review of this work. Primary Handling Editor: Carolina Ortiz Guerrero. A peer review file is available

**Reprints and permissions information** is available at <http://www.nature.com/reprints>

**Publisher's note** Springer Nature remains neutral with regard to jurisdictional claims in published maps and institutional affiliations.

**Open Access** This article is licensed under a Creative Commons Attribution-NonCommercial-NoDerivatives 4.0 International License, which permits any non-commercial use, sharing, distribution and reproduction in any medium or format, as long as you give appropriate credit to the original author(s) and the source, provide a link to the Creative Commons licence, and indicate if you modified the licensed material. You do not have permission under this licence to share adapted material derived from this article or parts of it. The images or other third party material in this article are included in the article's Creative Commons licence, unless indicated otherwise in a credit line to the material. If material is not included in the article's Creative Commons licence and your intended use is not permitted by statutory regulation or exceeds the permitted use, you will need to obtain permission directly from the copyright holder. To view a copy of this licence, visit <http://creativecommons.org/licenses/by-nc-nd/4.0/>.

© The Author(s) 2025